HHS Public Access

Author manuscript

Chem Eng J. Author manuscript; available in PMC 2019 September 15.

Published in final edited form as:

Chem Eng J. 2018 September 15; 348: 786–798. doi:10.1016/j.cej.2018.04.198.

In Situ Synthesis of Polyurethane Scaffolds with Tunable Properties by Controlled Crosslinking of Tri-Block Copolymer and Polycaprolactone Triol for Tissue Regeneration

Hao-Yang Mi[a,b,c], **Xin Jing**[a,b], **Galip Yilmaz**[a,c], **Breanna S. Hagerty**[c], **Eduardo Enriquez**[c], and **Lih-Sheng Turng**[a,c]

[a]Department of Mechanical Engineering University of Wisconsin–Madison, Madison, WI, 53706, USA

[b]Department of Industrial Equipment and Control Engineering, South China University of Technology, Guangzhou, 510640, China

[c]Wisconsin Institute for Discovery University of Wisconsin–Madison, Madison, Wisconsin, 53715, USA

Abstract

Mimicking the mechanical properties of native tissues is a critical criterion for an ideal tissue engineering scaffold. However, most biodegradable synthetic materials, including polyester-based polyurethanes (PUs), consist of rigid polyester chains and have high crystallinity. They typically lack the elasticity of most human tissues. In this study, a new type of biodegradable PU with excellent elasticity was synthesized based on the controlled crosslinking of poly(ester ether) triblock copolymer diols and polycaprolactone (PCL) triols using urethane linkages. Three-dimensional (3D) porous scaffolds with a defined geometry, tunable microstructures, and adjustable mechanical properties were synthesized *in situ* using an isocyanate-ended copolymer, a tri-armed PCL, and a chain extender. The mechanical properties of the scaffolds can be easily tuned by changing the ratio of reactants, varying the solution concentration, or using a porogen. Notably, all of these scaffolds, although mostly made of rigid PCL chains, showed remarkable elasticity and cyclical properties. With an optimized molecular design, a maximum recovery rate of 99.8% was achieved. This was because the copolymer provided molecular flexibility while the long chain crosslinking of PCL triol hindered crystallization, thus making the PU behave like an amorphous elastic material. Moreover, the *in vitro* cell culture of 3T3 fibroblasts and MG63 osteoblast-like cells confirmed the biocompatibility of these PU scaffolds and revealed that scaffolds with different stiffnesses can stimulate the proliferation of different types of cells. All of

Corresponding authors: Lih-Sheng Turng, Tel: 608-316-4310; turng@engr.wisc.edu; Xin Jing, Tel: 86-18578664293; xjing3@wisc.edu.

Supporting Information

Additional SEM images; Compression and tensile test results; Live/dead assay of control group; Cell morphology SEM on scaffolds; A movie showing the elastic property of synthesized PU scaffolds.

these attributes make PU scaffolds extremely suitable for the regeneration of tissues that experience dynamic loading.

Graphical abstract

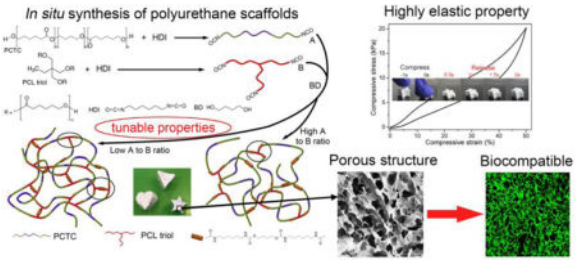

Keywords

Polyurethane; porous scaffolds; tissue engineering; tunable properties; elasticity

1. Introduction

Tissue engineering, which is an interdisciplinary field aimed at developing biological substitutes that restore, maintain, and/or improve tissue function, has been attracting considerable attention because it provides a way to develop artificial tissues as an alternative for autografts and allografts.[1, 2] In a typical tissue engineering process, the functional biomaterial—which is called the tissue engineering scaffold—plays a pivotal role in providing the substrate for cell growth and maintaining suitable mechanical properties during new tissue regeneration.[3] As this field of research approaches practical application, more requirements are raised for the scaffold materials. An ideal scaffold needs to have the following characteristics: (1) an interconnected porous structure that allows cell penetration and nutrition transportation, (2) suitable mechanical properties that mimic the surrounding tissue with sufficient mechanical support during the process, (3) biodegradability that allows new tissues to eventually take the place of the artificial scaffold, and (4) biocompatibility that facilitates cell attachment and proliferation.[4–6] In order to fulfill these requirements, researchers have focused on developing new materials and composite materials, as well as exploring novel scaffold fabrication methods.[7–9]

So far, many biocompatible and biodegradable synthetic materials have been proven capable of being used as tissue engineering scaffold materials for the regeneration of various tissues. For example, polymers like polylactic acid (PLA), polycaprolactone (PCL), poly(glycolic acid) (PGA), poly (lactic-co-glycolic acid) (PLGA), and polyhydroxybutyrate (PHB)—and their blends or block copolymers—have been used to fabricate scaffolds for tendon, nerve, bone, cartilage, muscle, and myocardial tissue engineering applications.[10–15] Although these scaffolds may support the growth of relevant tissue, they fail to mimic the mechanical properties of the target tissue since most human tissues and organs are relatively soft and elastic, and many experience dynamic loading. Meanwhile, all of these biomaterials are polyesters, which typically have high stiffnesses and very limited flexibility. PLA and PCL

have rigidities similar to bone,[16] but their flexibility and especially their recoverability are far less than tissues like skin, tendons, heart tissue, ligaments, and muscles.[17–19]

Polyurethane (PU) is a class of polymeric elastomers that is generally synthesized by step-growth polymerization of polyols with isocyanates and low molecular weight diols or diamine chain-extenders forming a segmented polymer containing soft segments (polyol chains) and hard segments (urethane chains).[20, 21] PUs have received tremendous attention in various fields due to the diversity of their chemical structures and their wide range of mechanical properties. [22] However, most elastomeric PUs are polyether based, which means that they are non-degradable, although they may have good biocompatibility. [23] In recent years, researchers have synthesized various biodegradable PUs using polyester diols as soft segments and demonstrated their potential applications as scaffold materials for cardiovascular tissue,[24] skin tissue,[25] bone tissue,[26] blood vessels,[27] nerve tissue, [28] and wound dressings[29]. PCL has been the most commonly used soft segment in biodegradable PU synthesis. Furthermore, the properties of PUs can be controlled by varying the ratio between the soft and hard segments.[30–32] However, these polyester-based PUs are still quite rigid due to the abundance of ester bonds and their high crystallinity as demonstrated in our previous work.[33] Although their stiffness can be reduced after being fabricated into porous scaffolds, their elasticity is still poor. In other words, the scaffolds tend to undergo permanent deformation under dynamic loading.[34]

One approach that has recently been used to enhance the flexibility of polyester-based PU is by employing blocked copolymers, which contain both polyester and polyether blocks as soft segments, to hinder the crystallization of polyester chains and provide mobility to the PU macromolecules.[35–37] Trinca et al. used a copolymer consisting of polyethylene glycol (PEG), PLA, and poly (trimethylene carbonate) (PTMC) blocks as soft segments to synthesize flexible PU.[38] The poly(caprolactone ethylene glycol) triblock copolymer (PCL-PEG-PCL) has also been used to synthesize soft PU with a modulus as low as 5 MPa. [39] Henry et al. synthesized soft PU using two types of poly diols (PHB for the crystalline segment and poly(caprolactone-co-glycolide) for the amorphous segment), yielding a PU that showed a modulus of about 8 MPa.[40] Although flexible scaffolds were produced, none of these studies reported cyclic mechanical properties.

In our previous work, polycaprolactone-block-polytetrahydrofuran-block–polycaprolactone (PCTC) tri-block copolymer and a degradable chain extender were used to synthesize PU intended for the regeneration of soft tissue. The material achieved a low modulus of 2.2 MPa and showed a high initial recovery rate of 95.3%, but these values decreased in repetitive loading and unloading cycles.[41] Moreover, the same degradation problem arose when the proportion of the polyether moiety was too high in the PU since these chains were not degradable *in vivo* and could only possibly be removed by metabolism. Therefore, developing biodegradable elastic tissue engineering scaffolds is a bottleneck for engineering artificial tissues that can closely mimic the mechanical properties of native elastic tissues such as skin, muscle, and cartilage.

Inspired by the high elasticity of human elastin, crosslinking sites were introduced in the PU molecular structure in this study. In a previous study, we found no improvement in elasticity

when the crosslinking sites were created between amide bonds in the hard segments using diisocyanate.[33] Thus, in this study, we used PCL triols in the synthesis of PU to introduce long chain crosslinking, which provided more flexibility to the molecular chains. Combined with the PCTC copolymer, we were able to synthesize a polyester-based elastomeric PU scaffold with an initial recovery rate as high as 99.8%.

We also proposed a method of fabricating three-dimensional (3D) porous scaffolds with tunable microstructures and mechanical properties. Component A, which is an isocyanate-ended PCTC, and component B, which is an isocyanate-ended PCL triol, were separately synthesized. They were then mixed at different ratios in dioxane, followed by adding butanediol as a chain extender. The scaffolds were easily obtained from the solution after curing and freeze-drying. By casting the solution into different molds before curing, scaffolds with various shapes could be made. In this method, the microstructures (e.g., porosity) and mechanical properties of the scaffolds could be controlled by changing the ratio between components A and B, as well as the solution concentration, or using a porogen. Most importantly, these scaffolds, although they consisted mostly of rigid PCL, had high elasticity, were highly compressible and recoverable. Moreover, the biocompatibility of these scaffolds was verified by culturing 3T3 fibroblasts and MG63 cells as a model for soft tissue and stiff tissue, respectively. It was also confirmed that low stiffness scaffolds stimulated fibroblast growth, while high stiffness scaffolds stimulated osteoblast-like cell growth, indicating that these scaffolds have a high potential to be used in the regeneration of tissues with various mechanical properties.

2. Materials and Methods

2.1 Materials

Reactant materials, including polycaprolactone (PCL) triol (PCL, M_n = 900), poly-caprolactone-block-polytetrahydrofuran-block-polycaprolactone copolymer (PCTC, M_w = 2000, equal polymerization degree for each block), hexamethylene diisocynate (HDI), 1,4-butanediol (BD), dibutyltin dilaurate (DBTDL), and sodium chloride (NaCl) as a porogen were purchased from Sigma–Aldrich. PCL triol, PCTC, and BD were vacuum dried at 75 °C for 2 h prior to use. HDI was dried using a 4Å molecular sieve and then vacuum distilled. NaCl particles were sieved to 100~250 μm in size. Anhydrous 1,4-dioxane, absolute ethanol, and isopropanol were purchased from Sigma–Aldrich and used as received. Deionized (DI) water was used throughout the experiment.

2.2 Synthesis of Component Materials

In component A synthesis, 0.002 mol of HDI and 10 μl of DBTDL were added to a dried three-neck flask containing 8 mL of dioxane under a nitrogen environment. The flask was heated to 60 °C, then 0.001 mol of PCTC diol was dissolved in 15 mL of dioxane and slowly added to the flask with mechanical stirring at 70 rpm. Isocyanate-ended PCTC was obtained after 3 h of reaction.

In component B synthesis, 0.001 mol of PCL triol dissolved in 5 mL of dioxane was slowly added to 0.003 mol of HDI dissolved in 1 mL of dioxane at 50 °C with magnetic stirring at 100 rpm for 3 h. Isocyanate-ended PCL triol was thus obtained.

2.3 In Situ Synthesis of Porous Scaffolds

For in situ synthesis of porous scaffolds, as illustrated in Figure 1, components A and B were added to a flask with a defined molar ratio (10:1, 5:1, 1:1, and 1:3) and quickly mixed with vigorous stirring. BD was added dropwise as a chain extender to connect the isocyanate groups. The molar ratio of BD was 11.5, 6.5, 2.5, and 1.8 times that of component B for A-B 10-1, A-B 5-1, A-B 1-1, and A-B 1-3, respectively. The resulting solution, which had a solid concentration of about 18%wt./vol., was mixed for 5 min and used to prepare the various scaffolds. The solution was then used in three different methods as follows: (1) directly casted to a Teflon mold, (2) diluted to 9%wt./vol. before casting by dioxane, and (3) casted to a polypropylene centrifuge tube filled with a NaCl porogen and centrifuged at 2000 rpm for 10 min to ensure solution penetration. Then the solutions were cured at 70 °C for 3 h, followed by being frozen at –80 °C and freeze-drying for 5 days. The scaffolds containing the NaCl porogens were leached in a circulating water bath for 2 days until they attained a constant weight. All scaffolds were immersed in 50% isopropanol for three days and dried in a desiccator prior to use. It is worth mentioning that, when a lower A to B ratio (e.g., 1:5) was used, the solution gelled too fast to be casted into the mold to form a regularly shaped scaffold.

2.4 Characterization of Chemical and Thermal Properties

The chemical structure of synthesized PUs was characterized by ^{1}H NMR (300 MHz, Bruker Biospin Co., Billerica, MA) using DMSO-d_6 (TMS, 99.9+%, NMR grade, Sigma–Aldrich) as a solvent with tetramethylsilane as an internal reference. Fourier transform infrared (FTIR) spectra were recorded in transmittance mode using a Bruker Tensor 27 spectrometer in the range of 4000–600 cm^{-1}, with a resolution of 4 cm^{-1}. The thermal properties were characterized via differential scanning calorimetry (DSC Q20, TA) and thermogravimetric analysis (TGA Q50, TA). DSC measurements were performed at a rate of 5 °C/min. Samples were first heated to 180 °C and then kept at 180 °C for 3 min to eliminate any prior thermal history, then cooled down to –100 °C and reheated to 180 °C. The TGA tests were initiated at room temperature and heated to 600 °C at a heating rate of 10 °C/min. The change in weight as the temperature increased was recorded.

2.5 Scaffold Morphology

Scanning electron microscopy (SEM) was used to characterize the morphological properties. Scaffolds were cryofractured in liquid nitrogen to expose undamaged porous structures and coated with a thin layer of gold, then imaged using a fully digital LEO GEMINI 1530 SEM (Zeiss, Germany) at a voltage of 3 kV. The pore sizes and pore densities of the scaffolds were measured from SEM images using the Image Pro-Plus software. The average pore diameter was calculated using Equation 1 to convert the surface average diameter to the volume average diameter.[42]

$$D^3 = \frac{1}{N}\sum_{i=1}^{N} D_i^3 \quad (1)$$

Equation 2 was used to calculate the volumetric pore density,

$$Pore\ density = \left(\frac{N}{A}\right)^{\frac{3}{2}} \quad (2)$$

where D_i is the diameter of an individual pore, N is the number of pores, and A is the area of the SEM image.

The porosities of the scaffolds were measured using a solvent replacement method.[43] Dried scaffolds were immersed in absolute ethanol for 2 h and weighed after excess ethanol on the surface was blotted. The porosity was calculated using Equation 3,

$$Porosity = (M_2 - M_1)/\rho V \quad (3)$$

where M_1 and M_2 are the mass of scaffolds before and after soaking in absolute ethanol, respectively; ρ is the density of absolute ethanol, and V is the volume of the scaffolds.

2.6 Mechanical Testing

The mechanical properties of fabricated PU scaffolds were measured on a universal mechanical testing machine (Instron 5967) at room temperature. Cylindrical samples were pre-wetted in phosphate-buffered saline (PBS) and compressed at a strain rate of 100%/min to 80% strain. Five samples were tested for each group and the compressive modulus and strength at 50% strain were measured. Samples were compressed and released at a strain rate of 100%/min to 50% strain for 10 cycles to evaluate their cyclic properties. The shape recovery rate in each cycle was calculated using Equation (4).[44] The hysteresis loss was measured from the area enclosed by the loading/unloading loop.

$$Recovery\ rate = \left(1 - \frac{L_{unloading}}{L_{loading}}\right) \times 100\% \quad (4)$$

where $L_{loading}$ and $L_{unloading}$ are the strains when the stress increases from zero or decreases to zero in the loading and unloading cycle, respectively.

Scaffolds were also compressed and released at a strain rate of 20%/min and 200%/min to investigate their recovery behavior under different stain rates.

2.7 *In Vitro* Degradation

The hydrolytic degradation behavior of synthesized PUs was investigated by PBS soaking. Briefly, PU scaffolds were hot compressed into discs at 150 °C and weighed individually to eliminate the effect of different porous structures. Samples were individually sealed in a plastic container filled with PBS solution, and then incubated at 37 °C on a parallel shaker (MaxQ 4000, Thermo Scientific) at a shaking rate of 225 rpm. The PBS was changed every 3 days to ensure a constant pH. The degradation test was performed for up to 10 weeks. At each time point, the samples were rinsed with DI water three times, followed by sufficient drying and weighing. The weight loss of the samples was calculated using Equation 5,

$$Weight\ loss = \left(1 - \frac{W_n}{W_o}\right) \times 100\% \quad (5)$$

where W_0 is the original sample weight and W_n is the weight of the same sample after degradation for a time period n.

2.8 3T3 and MG63 Cell Culture

NIH 3T3 fibroblasts and MG63 cells (Lonza) were cultured on the synthesized PU scaffolds to evaluate their cytotoxicity and cell proliferation. 3T3 and MG63 cells were pre-cultured on tissue culture-treated polystyrene flasks (BD Falcon) at a density of 5×10^5 cells/cm^2 in the same media after thawing at 37 °C with 5% CO_2 in air. The media contained Dulbecco's Modified Eagle's Medium (DMEM) (Invitrogen) supplemented with 20% fetal bovine serum (FBS, WiCell), 1% penicillin–streptomycin (10, 000 U/mL, Life Technologies), 1% L-glutamine (200 mM, Life Technologies), and 1% MEM non-essential amino acids (Life Technologies). When cells reached 70% confluency, they were passaged using TrypLE Express (Life Technologies).

Prior to cell seeding, scaffolds were washed with 20% ethanol six times and PBS solution twice to remove any impurities. The scaffolds were then UV sterilized for 1 h and placed in 24-well poly-HEMA treated non-attachable tissue culture plates. 3T3 and MG63 cells were treated with ethylenediaminetetraacetic acid (EDTA) for 5 min and washed with PBS solution, and then seeded on the samples separately at a cell density of 1.25×10^5 cells/cm^2. Spent medium was aspirated and replaced with 1 mL of fresh medium daily for screening samples. Samples were characterized at day 1, day 5, and day 10 time points. Cells were also cultured on tissue culture plates (TCPs) as control groups.

2.9 Biological Characterization

Cell viability was assessed via a Live/Dead viability/cytotoxicity kit (Life Technologies). The staining protocol followed the manufacturer's instructions. The green fluorescent calcein-AM was used to target the living cells, while the red fluorescence ethidium homodimer-1 (EthD-1) was used to indicate cell death. Stained cells were imaged with a Nikon A1 confocal microscope with a 488 nm laser and a 561 nm laser to detect green and red fluorescence, respectively. Nis-D Elements Advanced Research v.3.22 software was used for image analysis.

The number of cell on the scaffolds was evaluated using an MTS assay after culturing for 1 day, 5 days, and 10 days using the CellTiter 96 Aqueous One Solution kit (Promega Life Sciences). The whole procedure followed the manufacturer's instructions. Upon testing, cells were treated with media containing a 20% MTS solution and allowed to incubate for 1 h. Then, 100 μL of spent media were transferred into a clear 96-well plate. The absorbance of the plates at a 450 nm wavelength was read with a Glomax−Multi+Multiplate Reader (Promega). The subsequent number of cells was determined relative to a negative control.

2.10 Statistical Analysis

All biological results are presented as mean ± standard deviation. All of the values were averaged at least in triplicate. The data were analyzed using the one-way analysis of variance method (ANOVA). The Turkey's test was then used to evaluate the specific differences of the data, and these differences were considered statistically significant at $p < 0.05$.

3. Results and Discussion

3.1 Chemical Characterization of Synthesized PUs

In the synthesized PUs, as shown in Figure 2, component A was a linear tri-block copolymer ended with diisocyanate groups, component B was a tri-armed PCL ended with tri-isocyanate groups, and the isocyanate groups were linked with BD to form the hard segment in the PU. The crosslinking degree of the synthesized PU can be easily controlled by changing the ratio between A and B. With a high A to B ratio, junctions were mainly formed between linear chains, and crosslinking sites were mostly created between A and B components forming "T" junctions, as highlighted in the diagram. As the B component increased, the connection between components A and B decreased and the amount of "T" junctions increased. Moreover, when excess component B was present, the reaction between the tri-armed PCL formed "工" junctions, which are shorter and stiffer crosslinking sites than "T" junctions. Through this controlled crosslinking mechanism, the properties of synthesized scaffolds could be precisely altered and the elasticity could be improved.

The synthesized PUs were first characterized using ^{1}H NMR to verify their chemical structures. Although been crosslinked, the PUs were still able to dissolve in DMSO-d_6 at a concentration of 5 mg/mL to form a clear, gel-like solution. As shown in Figure 3, four PUs showed similar NMR patterns, thus implying similar chemical structures. However, the relative intensity for some of the peaks was different, thus indicating a difference in the number of specific chemical bonds. As depicted in the figure, the peak at 0.8 ppm was assigned to the methyl group of PCL triols, and it was higher for PUs with lower A to B ratios. The peaks between 1–2 ppm were assigned to the CH_2 group in PCL, PTHF, HDI, and BD. The peak at 2.9 ppm corresponded to the CH_2 adjacent to NH in the hard segment. [45] The peaks at 4.0 and 2.3 ppm were assigned to the protons adjacent to the carbon–oxygen single and double bonds in the ester group of PCL, respectively. The intensity of all of these peaks increased as the proportion of component B increased due to the introduction of more PCL and hard segments. Small peaks that belonged to the protons of NH and NH_2 were also detected. The amino groups were formed by the reaction of excess isocyanate

groups with water, which would provide bio-interactive sites with cells. The NMR results suggested the successful synthesis of the various PUs with different A to B ratios.

FTIR was further employed to confirm the chemical structure of synthesized PUs. As shown in Figure 4, four curves showed very similar peak patterns, but the relative intensity of the specific characteristic peaks differed among them. The absorption bands at 3327 cm^{-1} and 1697 cm^{-1} were ascribed to N–H and C–N stretching from amide bonds, respectively, suggesting the formation of urethane linkages.[46] The absorption bands at 1623 cm^{-1} and 1246 cm^{-1} corresponded to amide II and amide III in urethane, which provided strong evidence of the successful synthesis of PU.[47] The characteristic peaks located at 2933 cm^{-1} and 2859 cm^{-1} corresponded to the asymmetric and symmetric stretching vibrations of the $–CH_2$ groups.[47] Two distinct peaks at 1729 cm^{-1} and 1161 cm^{-1} were assigned to C=O and C–O–C bonds in the ester group of the PCL moiety, while the peak at 1105 cm^{-1} was ascribed to the C–O–C bond in the ether group of the PTHF moiety.[48]

As the content of component B increased, more urethane linkages formed as reflected by the increase of peak intensity of amide I, amide II, amide III, and N–H bonds. Meanwhile, the proportion of PTHF decreased as indicated by the intensity reduction at 1105 cm^{-1}. As more PCL and crosslinking sites were introduced, simultaneous improvements in mechanical properties and the recoverability of the scaffolds were expected.

3.2 Thermal Properties of Synthesized PUs

The high crystallinity and the presence of a vast number of ester bonds in most synthetic biomaterials, including polyester-based PUs, are the main reason for their high rigidity and low flexibility. These materials cannot withstand repetitive loading or deformation, thus, their mechanical properties are not ideal to match most human tissues. In our study, long chain crosslinking was introduced to the PU molecules to hinder the rearrangement of PCL chains and provide elasticity. DSC measurements were carried out to investigate the thermal behavior of the synthesized PUs. From the second heating scan (Figure 5a), it can be clearly seen that all materials showed a shallow glass transition slope at –56 to –59 °C, thus indicating the transition from a glassy state to a rubbery state. Composite A-B 10-1 showed a much larger and wider melting peak with an enthalpy of 24.2 J/g compared to other PUs with lower A to B ratios. The trend of crystallization peaks in the cooling cycle is consistent with the melting behavior (Figure 5b). This is strong evidence that an increase in crosslinking can effectively hinder the crystallization of PCL, although more PCL was introduced at the same time. The results indicate that PUs with lower A to B ratios actually behave more like an amorphous material. Another interesting finding is that both the melting temperature (T_m) and the crystallization temperature (T_c) decreased as the ratio of A to B decreased. However, these temperatures increased when the ratio was lower than 1:1. This might because the mobility of the molecular chains was hindered by the crosslinking sites, which made the crystalline region easier to melt and more difficult to form. However, as the B components increase further (e.g., A-B 1-3), the T_m and T_c start to approach that of PCL.[49]

The thermal degradation properties of PUs were investigated using TGA. As shown in Figure 6a, the onset decomposition temperature (T_d) increased from 232.8 °C for A-B 10-1

to 261.1 °C for A-B 1-3 as the content of component B increased. This can be attributed to the increased number of chemical crosslinking sites. The differentiation curves (Figure 6b) clearly showed the weight loss rate changes of each component in the material. For these PUs, the urethane linkages in the hard segment decomposed first, followed by the PCL moiety and PTHF moiety as the temperature increased.[50] It was found that the peak temperature of the PCL and PTHF moieties were about the same for four PUs, while the temperature assigned to the urethane linkages was higher for PUs with more B component. This further indicated that crosslinking postponed the thermal decomposition of hard segments in these PUs. The area under each peak reflects the proportion of each corresponding component in the material. It is obvious that the content of PCL and urethane increased while the PTHF content decreased as the A to B ratio decreased, which is in agreement with the NMR and FTIR results.

3.3 Morphology of PU Scaffolds

Twelve 3D cylindrical scaffolds with different microstructures were fabricated using four PUs (with different A to B ratios) via three different methods (i.e., direct casting at 18% wt./vol., dilution to 9% wt./vol. before casting, and casting with NaCl porogens) as previously discussed in Section 2.3. Figure 7 shows the morphologies and pore size distributions of these scaffolds. The pore size distribution was uniform showing a normal distribution for all scaffolds as depicted in the distribution histograms. Generally, it was found that scaffolds fabricated using 18% solution showed smaller pore sizes than those fabricated using 9% solution. Furthermore, the pore size was larger for the scaffolds made of PUs that had high A to B ratios. This was because smaller dioxane crystals were formed in PUs that had more crosslinking sites since their molecular chains were more difficult to rearrange. However, when a NaCl porogen was used in the fabrication, the pore size was about the same for all PUs. The thickness of the pore walls was less than 1 μm, and many pores were interconnected with each other, especially for those with larger diameters, as shown in Figure S1. The micro-channels among the pores are believed to be able to facilitate cell infiltration and nutrition transportation.[51, 52]

The statistical results of the average porosity, pore size, and pore density are shown in Figure 8, from which it was found that the structure of the scaffolds was mainly affected by the fabrication method. The scaffolds fabricated using the 18% solution had porosity values ranging from 45 to 80%, pore sizes from 5 to 15 μm, and pore densities from 30 to 260 × $10^5/cm^3$. The scaffolds fabricated using the 9% solution had porosity values from 80 to 94 %, pore sizes from 13 to 65 μm, and pore densities from 18 to 65 × $10^5/cm^3$. The scaffolds fabricated using NaCl as a porogen had porosities over 90%, pore sizes of about 175 μm, and pore densities of about 2.5 ×$10^4/cm^3$. Therefore, we were able to alter the microstructure of the 3D scaffolds easily by changing the fabrication method and the PU synthesis formula to meet the requirements of various tissues. Moreover, scaffolds with fine pores (< 20 μm) may also find applications as microcarriers for drug and protein delivery.[53, 54]

3.4 Mechanical Properties of PU Scaffolds

Mechanical performance is one of the most important properties for tissue engineering scaffolds, especially those intended for implantation for load bearing tissues. Synthetic materials such as PLA and PCL have been widely proven suitable for bone tissue engineering due to their high modulus and stiffness, which are similar to that of bone.[55–57] However, most human tissues, such as skin, heart, liver, muscle, and blood vessels, as well as ligament and cartilage, prefer elastic implants that have similar mechanical strengths, can withstand repetitive loading and unloading, and can maintain their shape and properties over time.[58]

The mechanical properties of various PU scaffolds synthesized in this study were characterized thoughtfully. The deformation of the PU scaffolds showed the three main regions as depicted in Figure 9a, a typical compression curve of the synthesized scaffolds. These regions can be divided into an initial linear elastic region where strain energy is stored in the reversible bending of pore the walls; a plateau region where the pore walls start to fold and collapse; and a densification region where the pore walls start stacking, causing the internal strength to increase rapidly. To avoid destruction of the scaffold structure, all scaffolds were compressed to 50% strain (below the densification region) for 10 cycles to evaluate their mechanical performance. Figures 9b and c showed that the compressive modulus and strength at 50% strain were higher for scaffolds made of PUs with lower A to B ratios and scaffolds with smaller pore sizes. For A-B 10-1 PU, the modulus ranged from 1.6 to 12.6 kPa, and the strength ranged from 0.7 to 9.3 kPa when fabricated into scaffolds using different methods. For different scaffolds fabricated using A-B 1-3 PU, the modulus increased to 45.0–244.8 kPa, and the strength improved to 23.7–141.1 kPa, depending on the method used. The wide mechanical property range of scaffolds we fabricated indicated their potential to be used in the regeneration of various types of elastic tissues. For example, human cerebral vein, ureter, vascular elastin, smooth muscle, and skin have moduli ranging from 10 to 700 kPa.[18, 59, 60] The cyclic compressive curves (Figure 9d) showed that the hysteresis loops, which reflect the loss of energy in each loading and unloading cycle, were different for scaffolds made of different PUs. The hysteresis loss is an indicator of energy dissipated in the loading/unloading cycle. It was found that the loop almost overlapped for scaffolds made of A-B 10-1 and A-B 5-1 PUs. However, the scaffolds made of A-B 5-1 and A-B 1-3 PUs had an obvious decrease in hysteresis loss in the first few cycles, and the loss gradually became constant in latter cycles, indicating good cyclical properties in the long term.

As shown in Figure 9e and Movie 1, the scaffold fully recovers gradually after being compressed to about 20% of its original height. This special elastic property can be attributed to the synergistic effect of flexible copolymer chains, crosslinking sites, and decreased PCL crystallinity. The recovery rate with respect to the original height of the scaffolds and the hysteresis loss in the first and tenth cycles were measured to investigate the recoverability. Figure 9f shows that the recovery rate was maintained over 10 cycles of loading and unloading, and it was lower for the scaffolds with larger porosities due to their higher void fractions. It was also found that the A-B 5-1 PU scaffolds showed the highest recovery rate (99.8% initial recovery rate), which was still over 98% after ten cycles of

cyclic compression. Figure 9g shows the hysteresis loss (energy dissipation) of the scaffolds in the first and tenth cycles. It was found that the hysteresis loss was higher for scaffolds with smaller pore sizes and scaffolds made of PUs with lower A to B ratios, thus indicating that stiffer scaffolds dissipated more energy in the cyclical test. The high elasticity of these PU scaffolds contributed to the synergetic effects of the incorporation of flexible copolymer chains, increased crosslinking, and decreased crystallinity as the A to B ratio decreased.

The scaffolds were also compressed at different strain rates to investigate their stain responses. As shown in Figure S2, at higher strain rates, both compressive strength and hysteresis loss were higher for all scaffolds, indicating the typical elastic deformation behavior for foams. Similar to the cyclical tests, A-B 10-1 and A-B 5-1 PUs showed small hysteresis losses and less of a difference under different strain rates, while A-B 1-1 and A-B 1-3 PUs showed an obvious increase in hysteresis loss when compressed at a higher rate, thus indicating more energy dissipation.

Besides compression, these scaffolds possessed high recoverability in tensile tests, as shown in Figure S3. Similar to compression tests, the scaffolds with a higher component B content showed superior Young's moduli and tensile strengths. The elongation-at-break of A-B 5-1 was the highest, indicating high flexibility. The cyclic tensile test showed that all scaffolds possessed excellent recoverability, with strain–stress curves overlapping within ten cycles. Similar to compression tests, scaffolds with higher component B content showed greater hysteresis losses. Thus, we demonstrated that the PU scaffolds synthesized in this study had remarkable elastic properties which can resemble the elasticity of many human tissues.

3.5 Biodegradation of PU scaffolds

The degradation of PU scaffolds was evaluated for up to 10 weeks by immersion in PBS at 37 °C with constant parallel shaking. Scaffolds were hot compressed into discs at 150 °C to minimize the effect of their porous structure. It was found in Figure 10 that the synthesized PUs showed relatively slow degradation rates, with a maximum 2.1% weight loss in 10 weeks as compared to some aliphatic polyesters like PLA, PLGA, and PGA.[61, 62] The results also indicated that the PUs that had lower A to B ratios had relatively faster degradation rates because the fraction of PTHF block (which is considered non-degradable) was lower. It has been reported that PCL loses 50% of its initial molecular weight after 12 months incubation in PBS,[63] and that it will break into pieces after *in vivo* degradation over 30 months.[64] PCL-based polyurethane takes about a year to reach a 50% reduction in molecular weight,[40] but it can be improved by adding hydrophilic moieties in the molecular design.[65] Moreover, the degradation rate of PCL-based PUs can be greatly enhanced in an enzymatic environment, such as proteinase and lipase enzymes.[22, 32, 66] Therefore, our PU scaffolds have comparable degradation rates with PCL and PCL-based PUs. As such, they have the potential to be used in the regeneration of slow-growing tissue, especially load-bearing tissue, since they should maintain their mechanical properties before they are substantially degraded over a long period of time.[46, 59]

3.6 Cytotoxicity of Fabricated PU Scaffolds to 3T3 and MG63 Cells

Two types of cells were cultured on PU scaffolds fabricated using 9% solution for up to 10 days to investigate the cytotoxicity and number of cells on scaffolds with different stiffness. 3T3 fibroblasts were cultured as a model of soft tissue for up to 10 days. Figure 11 shows the fluorescence images of the live/dead assays for different PU scaffolds. Green fluorescence indicates healthy live cells, while dead cells are labeled with red fluorescence. The statistical data of cell viability and cell population are shown in Figure 12. The number of cells and the cell viability significantly increased during 10 days of culture, and the cells showed a typical spindle-shape spread. At day 5, the cells almost covered the whole scaffold, especially on the A-B 10-1 scaffold. These results indicated that the PU scaffolds were biocompatible to 3T3 fibroblasts and provided a viable environment for cell growth. Comparing different scaffolds, it was interesting to find that both cell viability and cell proliferation were better on scaffolds made of PUs with higher A to B ratios. However, the cell population and viability on TCP was higher than that on the scaffolds, since TCP is usually treated with cell adhesion plasma (Figure S4). The SEM images showed that cells cultured on A-B 10-1 scaffolds had a larger cell area and a more spread-out cell morphology than those on A-B 1-3 scaffolds after 10 days of culture (Figure S5). This could be related to the modulus of the substrate since it has been reported that substrate stiffness has an effect on the cellular behavior of various cells, and even affects the differentiation of stem cells.[67, 68] From our results, it is obvious that soft scaffolds were more suitable for fibroblast growth as compared to relatively stiff scaffolds.

The fluorescence images and relative statistical data of MG63 cells cultured on different PU scaffolds are shown in Figures 13 and 14. MG63 is an osteosarcoma cell line that behaves similarly to osteoblasts and has been recognized as osteoblast-like cells.[69] The results indicate that these PU scaffolds were also suitable for MG63 cell growth as confirmed by about a five-fold increase in cell numbers and over 90% cell viability during the 10 days of culture. The MG63 cells presented a healthy spread growing state on all scaffolds, and the cell spreading area increased significantly from day 1 to day 10. When compared across different PU scaffolds, it was found that the cell population and cell viability on scaffolds with lower A to B ratios was higher than those with higher A to B ratios, and this difference was more obvious at day 5 and day 10. The cells cultured on scaffolds with lower A to B ratios formed larger cell membranes and showed better cell–substrate interactions as shown in the SEM images (Figure S6). This was also attributed to the high stiffness of the scaffolds with lower A to B ratios since it has been reported that osteoblasts have a strong dependence on substrate stiffness.[70] The *in vitro* culture results of 3T3 and MG63 cells verified that the PU scaffolds with different stiffness have good biocompatibility towards different types of cells. Furthermore, the dependence of cell proliferation on scaffold stiffness was also confirmed, which implies that these scaffolds are capable of being used in the regeneration of elastic tissues like skin, muscle, ureter, vein, and cartilage.

4. Conclusion

Regarding the lack of biodegradable flexible biomaterials for tissue engineering scaffold applications, a new type of highly elastic PU with tunable properties was synthesized based

on controlling the crosslinking of triblock copolymer diols and PCL triols. Porous tissue engineering scaffolds with defined shape, various porous structures and properties were fabricated through a simple in situ synthesis approach. The mechanical properties could be controlled by varying the ratio between the linear and branched polymer chains. The chemical structure and successful synthesis of PUs were confirmed by NMR and FTIR. The introduction of crosslinking sites hindered the crystallization of PCL chains and increased the thermal stability. The pore size and porosity of 3D porous scaffolds could be enhanced by reducing the solution concentration and using a NaCl porogen, and the PUs synthesized with higher A to B ratios had larger pore sizes. Most importantly, these PU scaffolds, although mostly made of rigid PCL chains, showed outstanding flexibility and recoverability, which can be attributed to the triblock copolymer and crosslinking sites created. The compressive moduli achieved by these scaffolds ranged from 45.0 to 244.8 kPa. When compressed, these scaffolds gradually recovered to their original shape with a recovery rate over 95%. The A-B 5-1 scaffolds achieved a maximum recovery rate of 99.8%. These scaffolds showed a relatively slow degradation rate with less than 2% weight loss over 10 weeks soaking in PBS, and the scaffolds containing more PCL moieties showed a faster degradation rate. These attributes made them extremely suitable for long term and cyclic load-bearing implantation situations. Moreover, *in vitro* cell culture of 3T3 fibroblast and MG63 cells confirmed the biocompatibility of these PU scaffolds and revealed that scaffolds with different stiffness could stimulate the proliferation of different types of cells. Therefore, these scaffolds have great potential to be used in the regeneration of various elastic tissues.

Supplementary Material

Refer to Web version on PubMed Central for supplementary material.

Acknowledgments

The research reported in this paper was partially supported by the NHLBI of the National Institutes of Health under award number U01HL134655. The content is solely the responsibility of the authors and does not necessarily represent the official views of the National Institutes of Health. The authors would also like to acknowledge the financial support of the National Natural Science Foundation of China (51603075; 21604026), the Kuo K. and Cindy F. Wang Professorship, the Wisconsin Institute for Discovery at the University of Wisconsin–Madison, and the University of Wisconsin-Madison Office of the Vice Chancellor for Research and Graduate Education with funding from the Wisconsin Alumni Research Foundation.

References

1. Langer R, Vacanti JP. Tissue Engineering. Science. 1993; 260:920–926. [PubMed: 8493529]
2. Wu SL, Liu XM, Yeung KWK, Liu CS, Yang XJ. Biomimetic porous scaffolds for bone tissue engineering. Mat Sci Eng R. 2014; 80:1–36.
3. Lee J, Cuddihy MJ, Kotov NA. Three-dimensional cell culture matrices: State of the art. Tissue Eng Pt B-Rev. 2008; 14:61–86.
4. Mi HY, Jing X, Turng LS. Fabrication of Bio-Based Cellular and Porous Materials for Tissue Engineering Scaffolds. In: Iannace S, Park CB, editorsBiofoams: Science and Applications of Bio-Based Cellular and Porous Materials. CRC Press; Boca Raton: 2015. 315–350.
5. Mandal BB, Kundu SC. Osteogenic and adipogenic differentiation of rat bone marrow cells on non-mulberry and mulberry silk gland fibroin 3D scaffolds. Biomaterials. 2009; 30:5019–5030. [PubMed: 19577292]

6. Hollister SJ. Porous scaffold design for tissue engineering. Nat Mater. 2005; 4:518–524. [PubMed: 16003400]
7. Mackova H, Plichta Z, Hlidkova H, Sedlacek O, Konefal R, Sadakbayeva Z, Duskova-Smrckova M, Horak D, Kubinova S. Reductively Degradable Poly(2-hydroxyethyl methacrylate) Hydrogels with Oriented Porosity for Tissue Engineering Applications. ACS Appl Mater Interfaces. 2017; 9:10544–10553. [PubMed: 28287694]
8. Okamoto M, John B. Synthetic biopolymer nanocomposites for tissue engineering scaffolds. Prog Polym Sci. 2013; 38:1487–1503.
9. Jing X, Mi HY, Wang XC, Peng XF, Turng LS. Shish-Kebab-Structured Poly(epsilon-Caprolactone) Nanofibers Hierarchically Decorated with Chitosan Poly(epsilon-Caprolactone) Copolymers for Bone Tissue Engineering. ACS Appl Mater Interfaces. 2015; 7:6955–6965. [PubMed: 25761418]
10. Place ES, George JH, Williams CK, Stevens MM. Synthetic polymer scaffolds for tissue engineering. Chem Soc Rev. 2009; 38:1139–1151. [PubMed: 19421585]
11. Kim IG, Hwang MP, Du P, Ko J, Ha CW, Do SH, Park K. Bioactive cell-derived matrices combined with polymer mesh scaffold for osteogenesis and bone healing. Biomaterials. 2015; 50:75–86. [PubMed: 25736498]
12. Chiono V, Tonda-Turo C. Trends in the design of nerve guidance channels in peripheral nerve tissue engineering. Prog Neurobiol. 2015; 131:87–104. [PubMed: 26093353]
13. Wang ZY, Teoh SH, Johana NB, Chong MSK, Teo EY, Hong MH, Chan JKY, Thian ES. Enhancing mesenchymal stem cell response using uniaxially stretched poly(epsilon-caprolactone) film micropatterns for vascular tissue engineering application. J Mater Chem B. 2014; 2:5898–5909.
14. Xu SJ, Liu JH, Zhang LC, Yang F, Tang PF, Wu DC. Effects of HAp and TCP in constructing tissue engineering scaffolds for bone repair. J Mater Chem B. 2017; 5:6110–6118.
15. Xie MH, Wang L, Guo BL, Wang Z, Chen YE, Ma PX. Ductile electroactive biodegradable hyperbranched polylactide copolymers enhancing myoblast differentiation. Biomaterials. 2015; 71:158–167. [PubMed: 26335860]
16. Igwe J, Amini A, Mikael P, Laurencin C, Nukavarapu S. Nanostructured Scaffolds for Bone Tissue Engineering. Stud Mechanobiol Tis. 2011; 8:169–192.
17. Folliguet TA, Rucker-Martin C, Pavoine C, Deroubaix E, Henaff M, Mercadier JJ, Hatem SN. Adult cardiac myocytes survive and remain excitable during long-term culture on synthetic supports. J Thorac Cardiov Sur. 2001; 121:510–519.
18. Serrano MC, Chung EJ, Ameer GA. Advances and Applications of Biodegradable Elastomers in Regenerative Medicine. Adv Funct Mater. 2010; 20:192–208.
19. Wu YB, Wang L, Zhao X, Hou S, Guo BL, Ma PX. Self-healing supramolecular bioelastomers with shape memory property as a multifunctional platform for biomedical applications via modular assembly. Biomaterials. 2016; 104:18–31. [PubMed: 27424213]
20. Mi HY, Salick MR, Jing X, Crone WC, Peng XF, Turng LS. Electrospinning of unidirectionally and orthogonally aligned thermoplastic polyurethane nanofibers: Fiber orientation and cell migration. J Biomed Mater Res A. 2015; 103:593–603. [PubMed: 24771704]
21. Lin HH, Hsieh FY, Tseng CS, Hsu SH. Preparation and characterization of a biodegradable polyurethane hydrogel and the hybrid gel with soy protein for 3D cell-laden bioprinting. J Mater Chem B. 2016; 4:6694–6705.
22. Chen J, Dong RN, Ge J, Guo BL, Ma PX. Biocompatible, Biodegradable, and Electroactive Polyurethane-Urea Elastomers with Tunable Hydrophilicity for Skeletal Muscle Tissue Engineering. ACS Appl Mater Interfaces. 2015; 7:28273–28285. [PubMed: 26641320]
23. Mi HY, Jing X, Salick MR, Cordie TM, Peng XF, Turng LS. Properties and fibroblast cellular response of soft and hard thermoplastic polyurethane electrospun nanofibrous scaffolds. J Biomed Mater Res B. 2015; 103:960–970.
24. Zhao X, Dong RN, Guo BL, Ma PX. Dopamine-Incorporated Dual Bioactive Electroactive Shape Memory Polyurethane Elastomers with Physiological Shape Recovery Temperature, High Stretchability, and Enhanced C2C12 Myogenic Differentiation. ACS Appl Mater Interfaces. 2017; 9:29595–29611. [PubMed: 28812353]

25. Karchin A, Simonovsky FI, Ratner BD, Sanders JE. Melt electrospinning of biodegradable polyurethane scaffolds. Acta Biomater. 2011; 7:3277–3284. [PubMed: 21640853]
26. Kavlock KD, Pechar TW, Hollinger JO, Guelcher SA, Goldstein AS. Synthesis and characterization of segmented poly(esterurethane urea) elastomers for bone tissue engineering. Acta Biomater. 2007; 3:475–484. [PubMed: 17418651]
27. Punnakitikashem P, Truong D, Menon JU, Nguyen KT, Hong Y. Electrospun biodegradable elastic polyurethane scaffolds with dipyridamole release for small diameter vascular grafts. Acta Biomater. 2014; 10:4618–4628. [PubMed: 25110284]
28. Wu YB, Wang L, Guo BL, Shao YP, Ma PX. Electroactive biodegradable polyurethane significantly enhanced Schwann cells myelin gene expression and neurotrophin secretion for peripheral nerve tissue engineering. Biomaterials. 2016; 87:18–31. [PubMed: 26897537]
29. Wang YF, Li PF, Xiang P, Lu JT, Yuan J, Shen J. Electrospun polyurethane/keratin/AgNP biocomposite mats for biocompatible and antibacterial wound dressings. J Mater Chem B. 2016; 4:635–648.
30. Heijkants RGJC, van Calck RV, van Tienen TG, de Groot JH, Buma P, Pennings AJ, Veth RPH, Schouten AJ. Uncatalyzed synthesis, thermal and mechanical properties of polyurethanes based on poly(epsilon-caprolactone) and 1,4-butane diisocyanate with uniform hard segment. Biomaterials. 2005; 26:4219–4228. [PubMed: 15683644]
31. Guan J, Sacks MS, Beckman EJ, Wagner WR. Synthesis, characterization, and cytocompatibility of elastomeric, biodegradable poly(ester-urethane)ureas based on poly(caprolactone) and putrescine. Journal of biomedical materials research. 2002; 61:493–503. [PubMed: 12115475]
32. Fang J, Ye SH, Shankarraman V, Huang YX, Mo XM, Wagner WR. Biodegradable poly(ester urethane)urea elastomers with variable amino content for subsequent functionalization with phosphorylcholine. Acta Biomater. 2014; 10:4639–4649. [PubMed: 25132273]
33. Mi HY, Jing X, Hagerty BS, Chen G, Huang A, Turng LS. Post-crosslinkable biodegradable thermoplastic polyurethanes: Synthesis, and thermal, mechanical, and degradation properties. Mater Des. 2017; 127:106–114.
34. Dey J, Xu H, Shen JH, Thevenot P, Gondi SR, Nguyen KT, Sumerlin BS, Tang LP, Yang J. Development of biodegradable crosslinked urethane-doped polyester elastomers. Biomaterials. 2008; 29:4637–4649. [PubMed: 18801566]
35. John JV, Moon BK, Kim I. Influence of soft segment content and chain length on the physical properties of poly(ether ester) elastomers and fabrication of honeycomb pattern and electrospun fiber. React Funct Polym. 2013; 73:1213–1222.
36. Henry JA, Burugapalli K, Neuenschwander P, Pandit A. Structural variants of biodegradable polyesterurethane in vivo evoke a cellular and angiogenic response that is dictated by architecture. Acta Biomater. 2009; 5:29–42. [PubMed: 18823827]
37. Deng ZX, Guo Y, Zhao X, Li LC, Dong RN, Guo BL, Ma PX. Stretchable degradable and electroactive shape memory copolymers with tunable recovery temperature enhance myogenic differentiation. Acta Biomater. 2016; 46:234–244. [PubMed: 27640917]
38. Trinca RB, Abraham GA, Felisberti MI. Electrospun nanofibrous scaffolds of segmented polyurethanes based on PEG, PLLA and PTMC blocks: Physico-chemical properties and morphology. Mat Sci Eng C-Mater. 2015; 56:511–517.
39. Guan JJ, Sacks MS, Beckman EJ, Wagner WR. Biodegradable poly(ether ester urethane)urea elastomers based on poly(ether ester) triblock copolymers and putrescine: synthesis, characterization and cytocompatibility. Biomaterials. 2004; 25:85–96. [PubMed: 14580912]
40. Henry JA, Simonet M, Pandit A, Neuenschwander P. Characterization of a slowly degrading biodegradable polyesterurethane for tissue engineering scaffolds. J Biomed Mater Res A. 2007; 82A:669–679.
41. Mi HY, Jing X, Napiwocki BN, Hagerty BS, Chen GJ, Turng LS. Biocompatible, degradable thermoplastic polyurethane based on polycaprolactone-block-polytetrahydrofuran-block-polycaprolactone copolymers for soft tissue engineering. J Mater Chem B. 2017; 5:4137–4151. [PubMed: 29170715]

42. Mi HY, Salick MR, Jing X, Jacques BR, Crone WC, Peng XF, Turng LS. Characterization of thermoplastic polyurethane/polylactic acid (TPU/PLA) tissue engineering scaffolds fabricated by microcellular injection molding. Mat Sci Eng C-Mater. 2013; 33:4767–4776.
43. Yin LC, Fei LK, Cui FY, Tang C, Yin CH. Superporous hydrogels containing poly(acrylic acid-co-acrylamide)/O-carboxymethyl chitosan interpenetrating polymer networks. Biomaterials. 2007; 28:1258–1266. [PubMed: 17118443]
44. Mi HY, Jing X, Politowicz AL, Chen E, Huang HX, Turng LS. Highly compressible ultra-light anisotropic cellulose/graphene aerogel fabricated by bidirectional freeze drying for selective oil absorption. Carbon. 2018; 132:199–209.
45. Nair PA, Ramesh P. Electrospun biodegradable calcium containing poly(ester-urethane)urea: Synthesis, fabrication, in vitro degradation, and biocompatibility evaluation. J Biomed Mater Res A. 2013; 101:1876–1887. [PubMed: 23712992]
46. Guelcher SA, Gallagher KM, Didier JE, Klinedinst DB, Doctor JS, Goldstein AS, Wilkes GL, Beckman EJ, Hollinger JO. Synthesis of biocompatible segmented polyurethanes from aliphatic diisocyanates and diurea diol chain extenders. Acta Biomater. 2005; 1:471–484. [PubMed: 16701828]
47. Zhang LS, Huang MM, Yu RL, Huang JC, Dong X, Zhang RY, Zhu J. Bio-based shape memory polyurethanes (Bio-SMPUs) with short side chains in the soft segment. J Mater Chem A. 2014; 2:11490–11498.
48. Chiono V, Mozetic P, Boffito M, Sartori S, Gioffredi E, Silvestri A, Rainer A, Giannitelli SM, Trombetta M, Nurzynska D, Di Meglio F, Castaldo C, Miraglia R, Montagnani S, Ciardelli G. Polyurethane-based scaffolds for myocardial tissue engineering. Interface Focus. 2014; 4
49. Mi HY, Jing X, Peng J, Salick MR, Peng XF, Turng LS. Poly(epsilon-caprolactone) (PCL)/cellulose nano-crystal (CNC) nanocomposites and foams. Cellulose. 2014; 21:2727–2741.
50. Zhang Y, Liao JJ, Fang XC, Bai FD, Qiao K, Wang LM. Renewable High-Performance Polyurethane Bioplastics Derived from Lignin-Poly(epsilon-caprolactone). Acs Sustain Chem Eng. 2017; 5:4276–4284.
51. Mi HY, Jing X, Salick MR, Turng LS, Peng XF. Fabrication of thermoplastic polyurethane tissue engineering scaffold by combining microcellular injection molding and particle leaching. J Mater Res. 2014; 29:911–922.
52. Jing X, Mi HY, Cordie T, Salick M, Peng XF, Turng LS. Fabrication of Porous Poly(e-caprolactone) Scaffolds Containing Chitosan Nanofibers by Combining Extrusion Foaming, Leaching, and Freeze-Drying Methods. Ind Eng Chem Res. 2014; 53:17909–17918.
53. Doty AC, Weinstein DG, Hirota K, Olsen KF, Ackermann R, Wang Y, Choi S, Schwendeman SP. Mechanisms of in vivo release of triamcinolone acetonide from PLGA microspheres. J Control Release. 2017; 256:19–25. [PubMed: 28342981]
54. Boyan BD, Lohmann CH, Somers A, Niederauer GG, Wozney JM, Dean DD, Carnes DL, Schwartz Z. Potential of porous poly-D,L-lactide-co-glycolide particles as a carrier for recombinant human bone morphogenetic protein-2 during osteoinduction in vivo. Journal of biomedical materials research. 1999; 46:51–59. [PubMed: 10357135]
55. Zhou CJ, Shi QF, Guo WH, Terrell L, Qureshi AT, Hayes DJ, Wu QL. Electrospun Bio-Nanocomposite Scaffolds for Bone Tissue Engineering by Cellulose Nanocrystals Reinforcing Maleic Anhydride Grafted PLA. ACS Appl Mater Interfaces. 2013; 5:3847–3854. [PubMed: 23590943]
56. Bose S, Vahabzadeh S, Bandyopadhyay A. Bone tissue engineering using 3D printing. Mater Today. 2013; 16:496–504.
57. Yao Q, Cosme JGL, Xu T, Miszuk JM, Picciani PHS, Fong H, Sun H. Three dimensional electrospun PCL/PLA blend nanofibrous scaffolds with significantly improved stem cells osteogenic differentiation and cranial bone formation. Biomaterials. 2017; 115:115–127. [PubMed: 27886552]
58. Mondschein RJ, Kanitkar A, Williams CB, Verbridge SS, Long TE. Polymer structure-property requirements for stereolithographic 3D printing of soft tissue engineering scaffolds. Biomaterials. 2017; 140:170–188. [PubMed: 28651145]

59. Agache PG, Monneur C, Leveque JL, De Rigal J. Mechanical properties and Young's modulus of human skin in vivo. Archives of dermatological research. 1980; 269:221–232. [PubMed: 7235730]
60. Liu QY, Jiang L, Shi R, Zhang LQ. Synthesis, preparation, in vitro degradation, and application of novel degradable bioelastomers-A review. Prog Polym Sci. 2012; 37:715–765.
61. Nair LS, Laurencin CT. Biodegradable polymers as biomaterials. Prog Polym Sci. 2007; 32:762–798.
62. Seal BL, Otero TC, Panitch A. Polymeric biomaterials for tissue and organ regeneration. Mat Sci Eng R. 2001; 34:147–230.
63. Cohn D, Salomon AF. Designing biodegradable multiblock PCL/PLA thermoplastic elastomers. Biomaterials. 2005; 26:2297–2305. [PubMed: 15585232]
64. Sun HF, Mei L, Song CX, Cui XM, Wang PY. The in vivo degradation, absorption and excretion of PCL-based implant. Biomaterials. 2006; 27:1735–1740. [PubMed: 16198413]
65. Guelcher SA. Biodegradable polyurethanes: Synthesis and applications in regenerative medicine. Tissue Eng Part B-Re. 2008; 14:3–17.
66. Daemi H, Rajabi-Zeleti S, Sardon H, Barikani M, Khademhosseini A, Baharvand H. A robust super-tough biodegradable elastomer engineered by supramolecular ionic interactions. Biomaterials. 2016; 84:54–63. [PubMed: 26803411]
67. Chaudhuri O, Gu L, Darnell M, Klumpers D, Bencherif SA, Weaver JC, Huebsch N, Mooney DJ. Substrate stress relaxation regulates cell spreading. Nat Commun. 2015; 6
68. Mao AS, Shin JW, Mooney DJ. Effects of substrate stiffness and cell-cell contact on mesenchymal stem cell differentiation. Biomaterials. 2016; 98:184–191. [PubMed: 27203745]
69. Tsai SW, Liaw JW, Kao YC, Huang MY, Lee CY, Rau LR, Huang CY, Wei KC, Ye TC. Internalized Gold Nanoparticles Do Not Affect the Osteogenesis and Apoptosis of MG63 Osteoblast-Like Cells: A Quantitative, In Vitro Study. Plos One. 2013; 8
70. Olivares-Navarrete R, Lee EM, Smith K, Hyzy SL, Doroudi M, Williams JK, Gall K, Boyan BD, Schwartz Z. Substrate Stiffness Controls Osteoblastic and Chondrocytic Differentiation of Mesenchymal Stem Cells without Exogenous Stimuli. Plos One. 2017; 12

Highlights

1. Synthesis elastic polycaprolactone based polyurethane by controlled crosslinking
2. Varying ratio between triblock copolymer and tri-armed PCL led to tunable properties
3. Porous 3D scaffolds can be *in situ* synthesized by simple mixing and curing method
4. All scaffolds possess high elasticity and recoverability (over 99.5%)
5. 3T3 and MG63 showed stiffness dependent proliferation on scaffolds with different properties

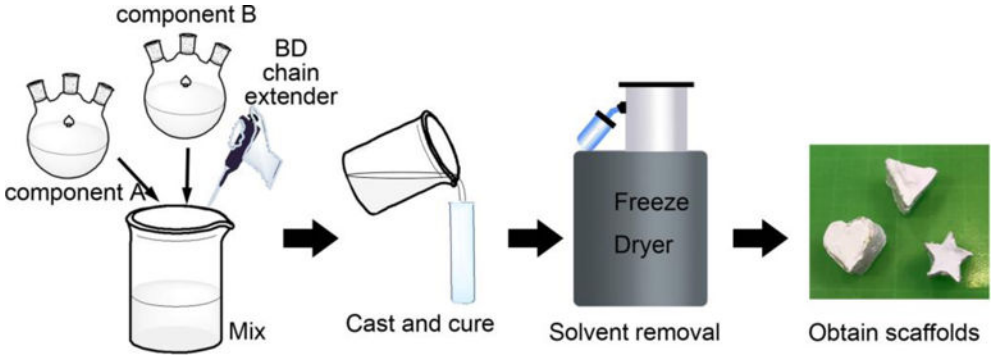

Figure 1.

Schematic of in situe scaffold synthesis. Components A and B, as well as BD, were added together at a defined molar ratio. Additional dioxane was added to adjust the concentration. The solution was then mixed and casted into molds with various cavities followed by curing and freeze drying to obtain porous scaffolds with different shapes.

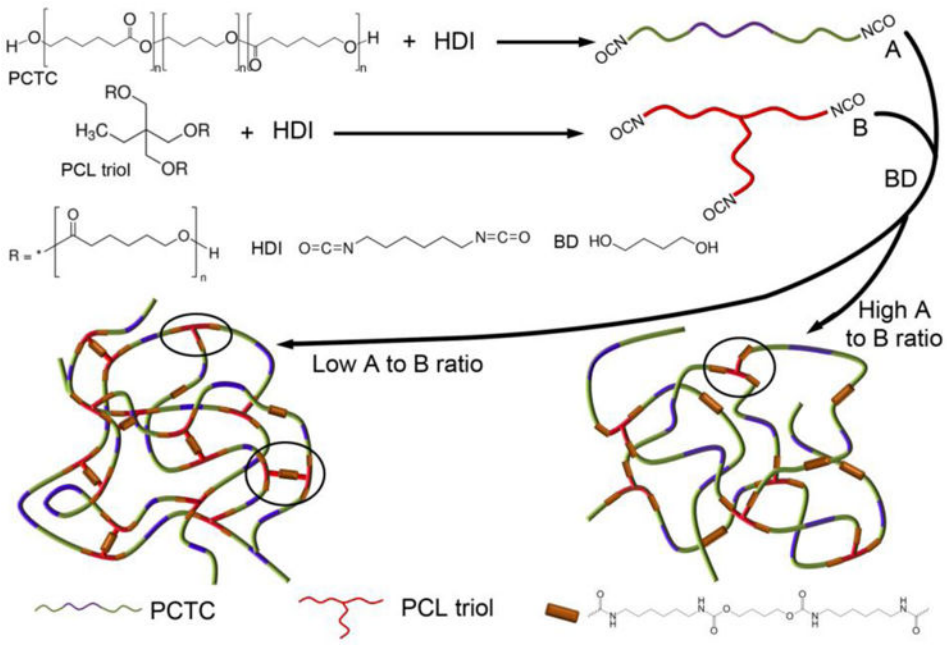

Figure 2.
Schematic showing the synthesis route of components A and B, and the controlled crosslinking of PUs by varying the A to B ratio.

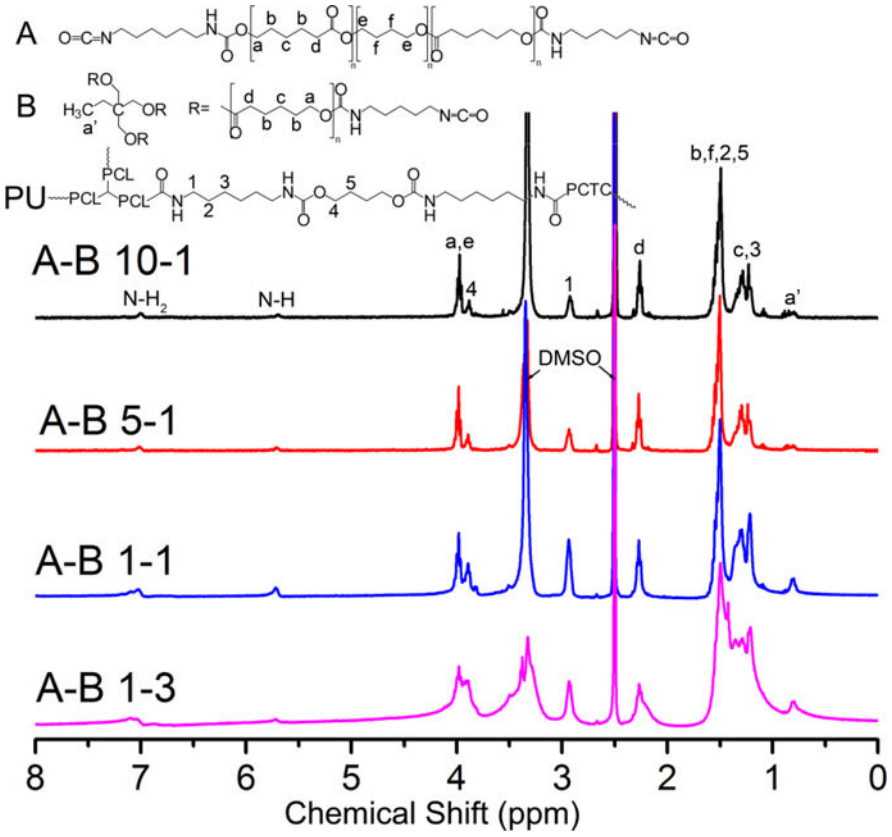

Figure 3.
^{1}H NMR results of synthesized PU with different A to B ratios.

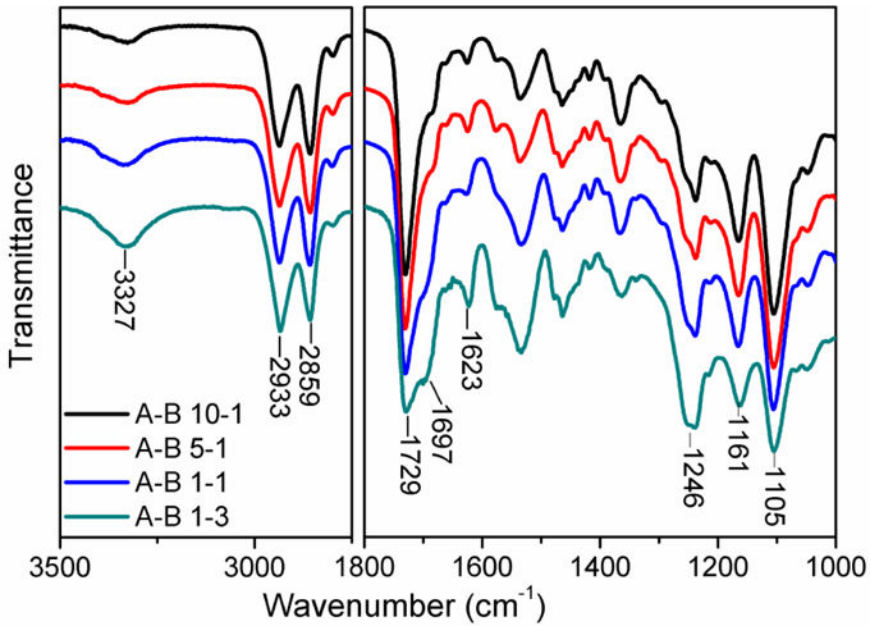

Figure 4.
FTIR results of synthesized PUs with different A to B ratios.

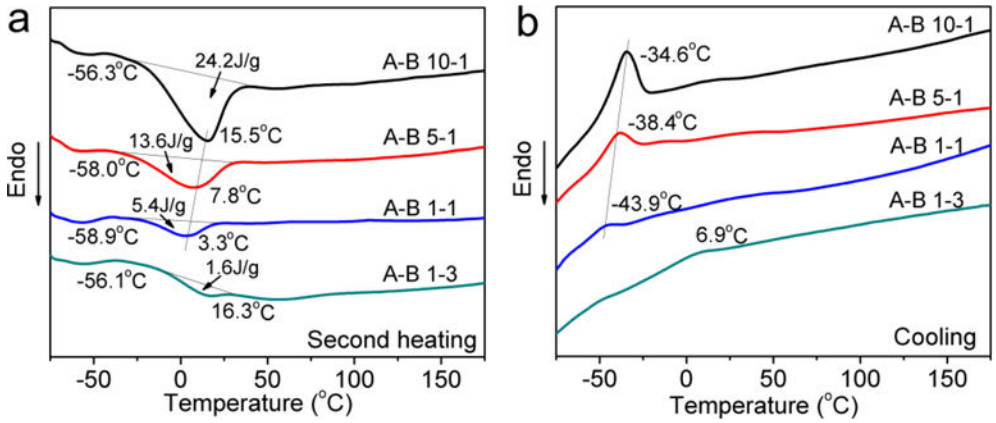

Figure 5.

DSC results of synthesized PUs with different A to B ratios. a) Second heating scan. b) Cooling scan.

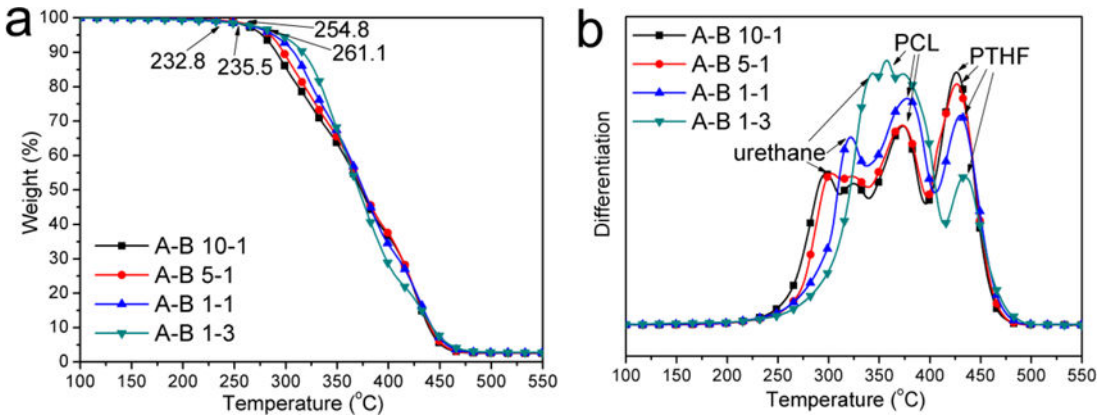

Figure 6.

TGA results of synthesized PUs with different A to B ratios: a) weight loss curves and b) differentiation curves.

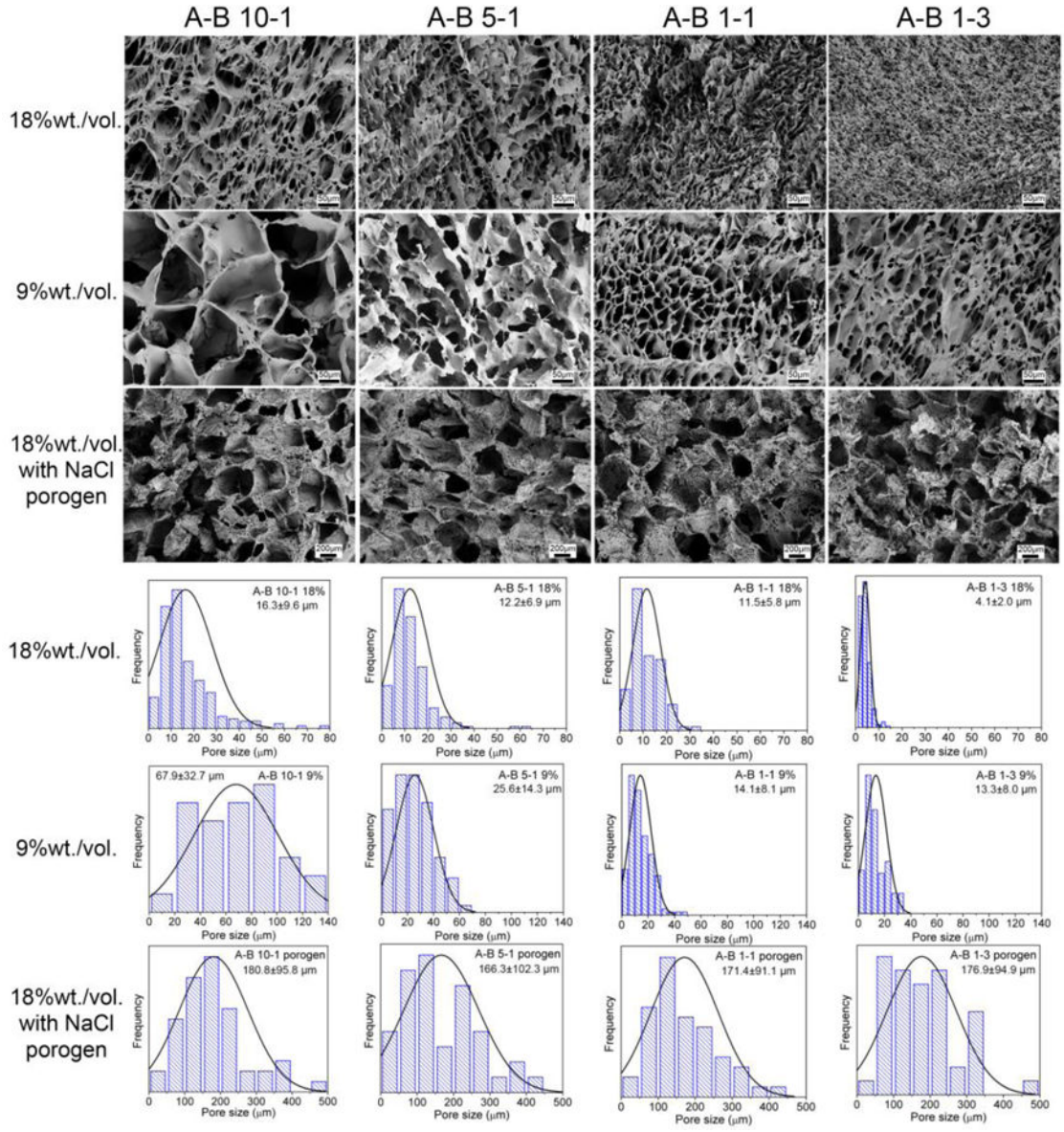

Figure 7.

Microstructure and corresponding pore size distribution results of fabricated PU scaffolds using PUs with different A to B ratios with 18% and 9% solution concentrations and with NaCl porogen. Scale bars for 18% and 9% scaffolds are 50 μm. Scale bars for scaffolds with NaCl porogen are 200 μm. The normal distribution curves are also plotted on the histograms.

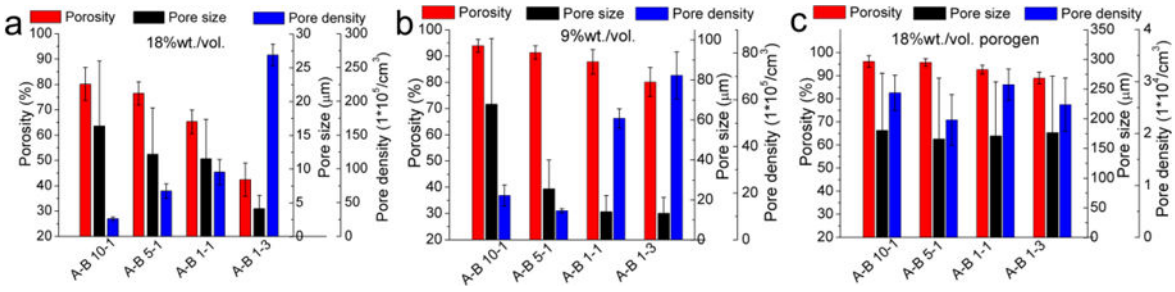

Figure 8.

Statistical results of the average porosity, pore size, and pore density of fabricated PU scaffolds using PUs with different A to B ratios. a) Scaffolds prepared using 18% solution, b) scaffolds prepared using 9% solution, and c) scaffolds prepared using NaCl porogen.

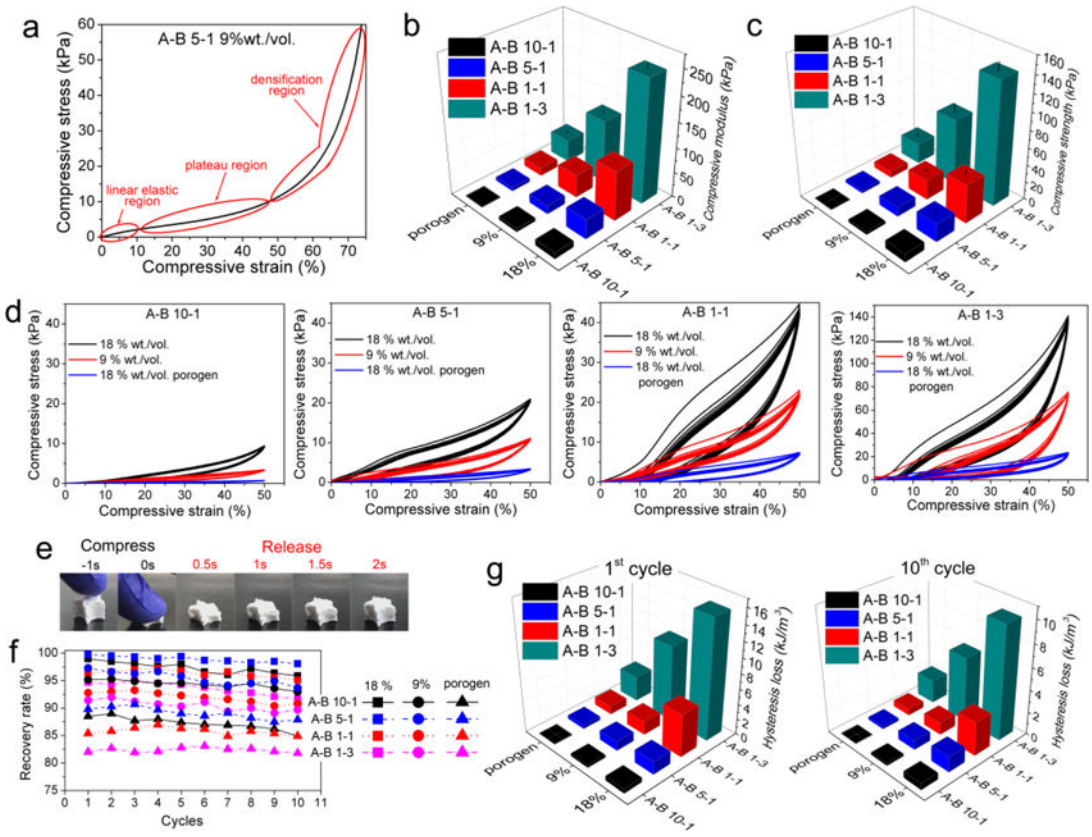

Figure 9.

Compression and cyclic compression properties of different PU scaffolds. a) A representative compression curve of the scaffolds. b) Compressive modulus and c) compressive strength at 50% strain statistical results. d) Cyclic compression test for 10 cycles. e) Demonstration of the elastic property of PU scaffolds. f) Recovery rate and g) hysteresis loss for different PU scaffolds in the first and tenth cycles.

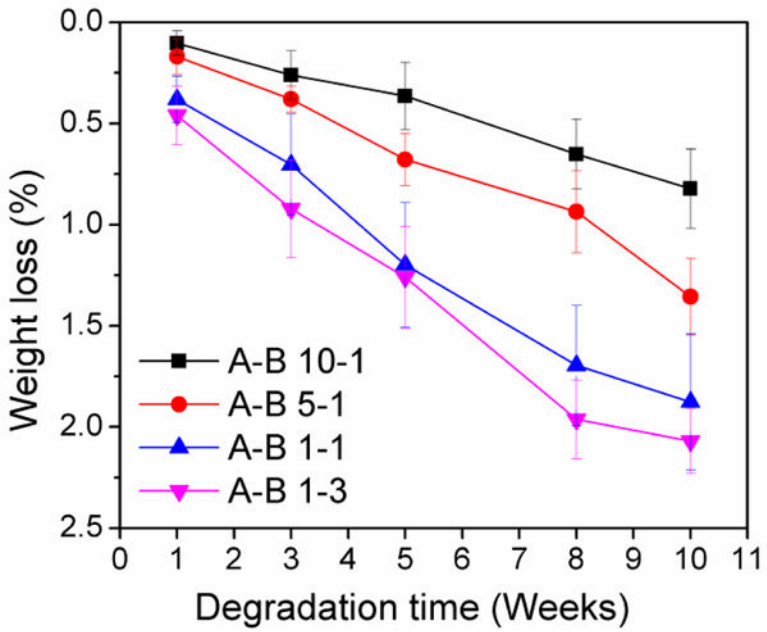

Figure 10.
Degradation results of synthesized PUs in PBS for up to 10 weeks.

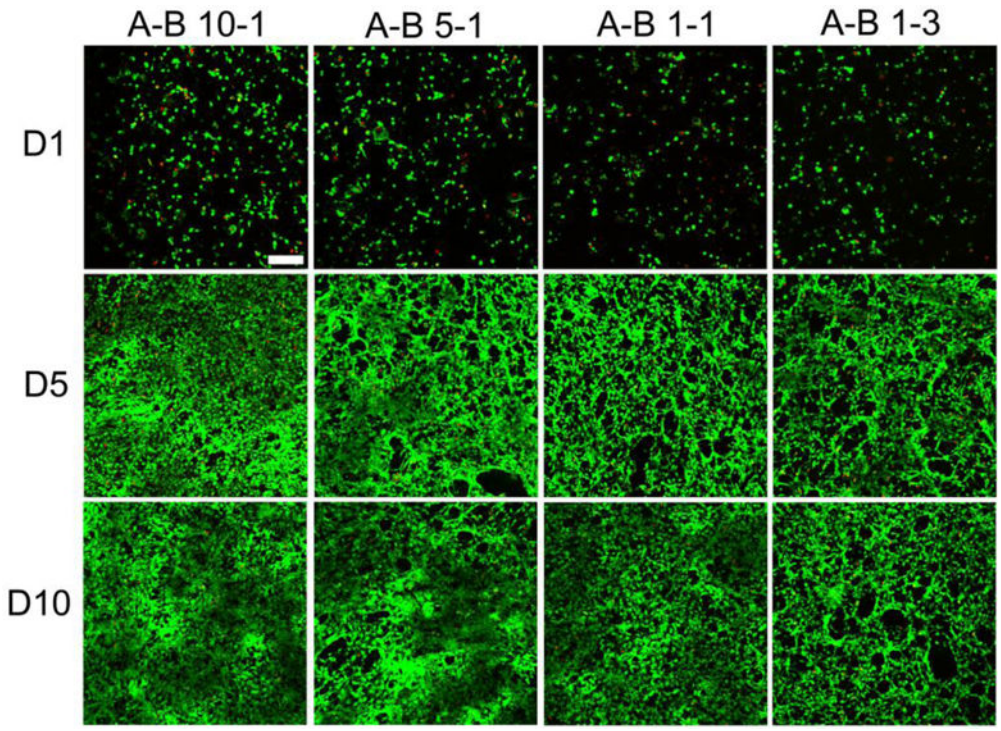

Figure 11.

Fluorescence images of live/dead assay results at day 1, day 5, and day 10 for 3T3 fibroblasts cultured on different PU scaffolds. Scale bar = 200 μm.

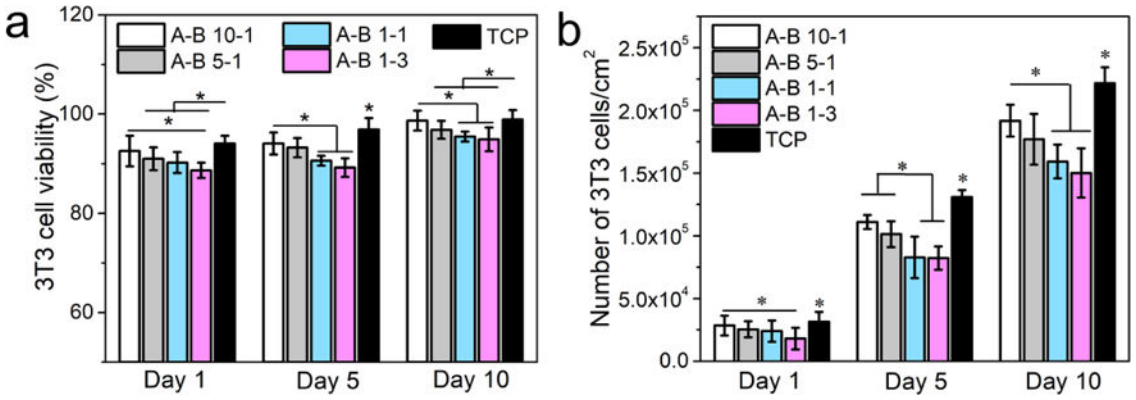

Figure 12.

3T3 fibroblast cell culture results on different PU scaffolds. a) Cell viability results from a live/dead assay, b) cell proliferation results from the MTS assay ($p < 0.05$).

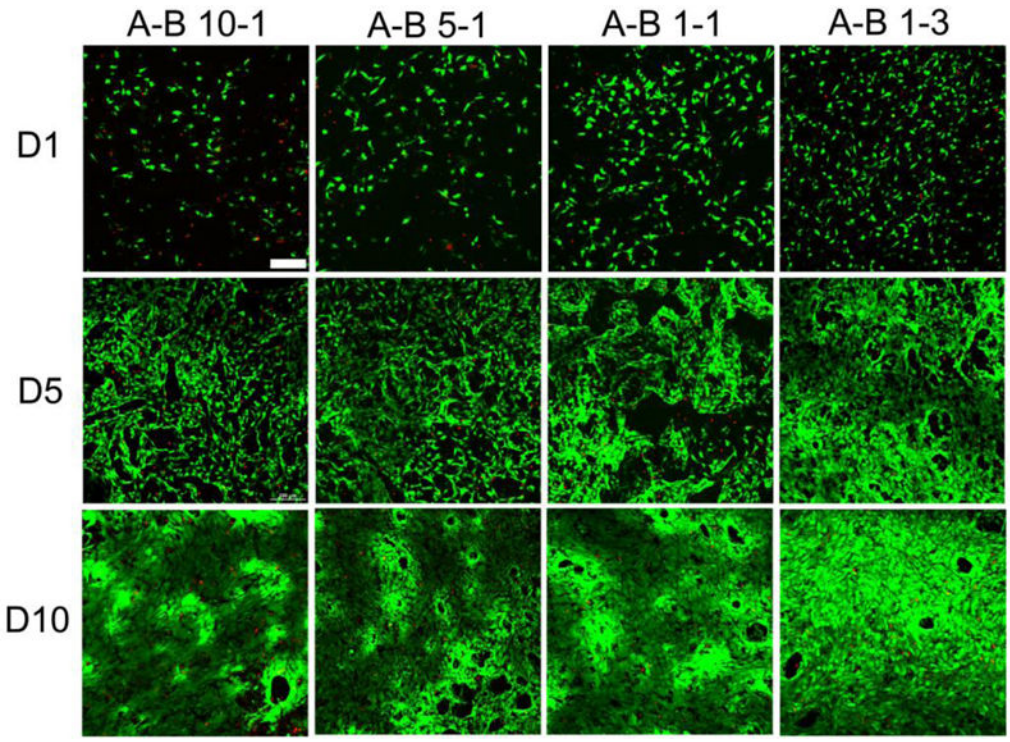

Figure 13.

Fluorescence images of live/dead assay results at day 1, day 5, and day 10 for MG63 cells cultured on different PU scaffolds. Scale bar = 200 μm.

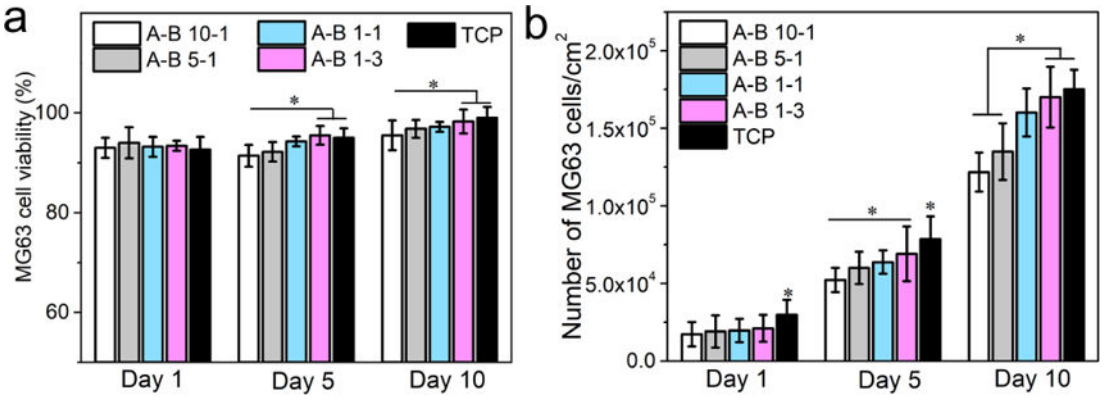

Figure 14.

MG63 cell culture results on different PU scaffolds and TCP. a) Cell viability results from the live/dead assay, and b) cell proliferation results from MTS assay ($p < 0.05$).